Towards high speed, low voltage electro-optical modulators in a foundry-process thin-film lithium niobate platform

Alberto Della Torre*, Ivan Prieto, Arno Mettraux, Homa Zarebidaki, Jacopo Leo, Michel Despont, Hamed Sattari
Swiss Center for Electronics and Microtechnology (CSEM), Neuchatel, Switzerland
*alberto.dellatorre@csem.ch.

ABSTRACT

We report on the performances of thin-film lithium niobate Mach-Zender electro-optical modulators manufactured using our standard foundry process and operating in the telecom C-band. We developed standard electro-optical modulators exhibiting a half-wave voltage of 3.2 V and an electro-optic bandwidth extending beyond 50 GHz. As a complementary option, we report CMOS voltage level folded modulators with half-wave voltage down to below 1 V, and bandwidths ranging from 8 to 25 GHz.

Keywords: Photonic integrated circuits, thin-film lithium niobate, electro-optical modulators, foundry process

1. INTRODUCTION

The escalating demand for swift data transmission and energy-efficient systems propels the evolution of Photonic Integrated Circuits (PICs). Key to achieving rapid and precise control of optical signals in modern telecommunications are high-speed electro-optical (EO) modulators. Simultaneously, the ability to manipulate light phase and amplitude using CMOS-level voltages presents a significant advantage for integrating PIC systems with less complex electrical ICs, thereby reducing overall power consumption. The potential applications extend beyond telecommunications, where modules operating with high bandwidth or low voltage could address diverse needs. Among various PIC platforms, Thin-film lithium niobate on insulator (TFLN) technology emerges as a standout performer. TFLN offers distinctive properties, including a broad transparency range, minimal optical loss, and a high electro-optic coefficient [1]. In contrast to alternative approaches like plasma dispersion effect [2], thermo-optics [3], MEMS [4], and plasmonics [5] in materials such as silicon, InP, and polymers, TFLN's exceptional EO properties promise superior solutions. These solutions have the potential to deliver low-voltage, low-power, and high-speed modulation [6]. Consequently, TFLN becomes a natural choice for developing efficient optical modulators, positioned to strike a balance in the conventional trade-off between high bandwidth and low voltage operations.
Here we report on the performances of TFLN Mach-Zender EO modulators (MZM) manufactured using our standard foundry process. We developed standard MZM with an EO bandwidth extending beyond 50 GHz. In addition, we report low voltage folded modulators in a compact 5mm × 5mm chip, potentially enabling to drive the device with fully integrated CMOS electrical circuits, without the need of off-chip amplification. The success of these devices serves as a validation of our standard fabrication process.

2. TFLN TECHNOLOGY

The devices are fabricated in a 150 mm wafer scale standard foundry process at CSEM. A schematical cross-sectional illustration of our TFLN PIC is presented in Figure 1(a). Our fabrication technology is based on commercially available thin film LNOI wafers which consist of a stack with 600 nm thick mono-crystal x-cut $LiNbO_3$ layer on top of a 4.7 µm buried thermal oxide (BOX) layer. The platform offers three distinct types of waveguides, thereby granting designers the flexibility to create circuits optimized for different wavelengths. This PIC platform features two metallization layers connected by a VIA. This structure enhances the radio frequency routing process, providing a more efficient path for signal transmission. In the platform, all layers are protected by a silicon oxide cladding. Then, a specialized layer, referred to as "clad open", is incorporated to provide designers the option to selectively remove the cladding. This feature allows for

specific applications, such as creating access points to the metal pads or directly interfacing with the waveguides. The final chip release process yields to smooth facets which are crucial for achieving efficient light coupling at both the input and output interfaces of the device. Figures 1(b) and 1(c) show SEM images of the edge couplers and of a MZM, respectively.

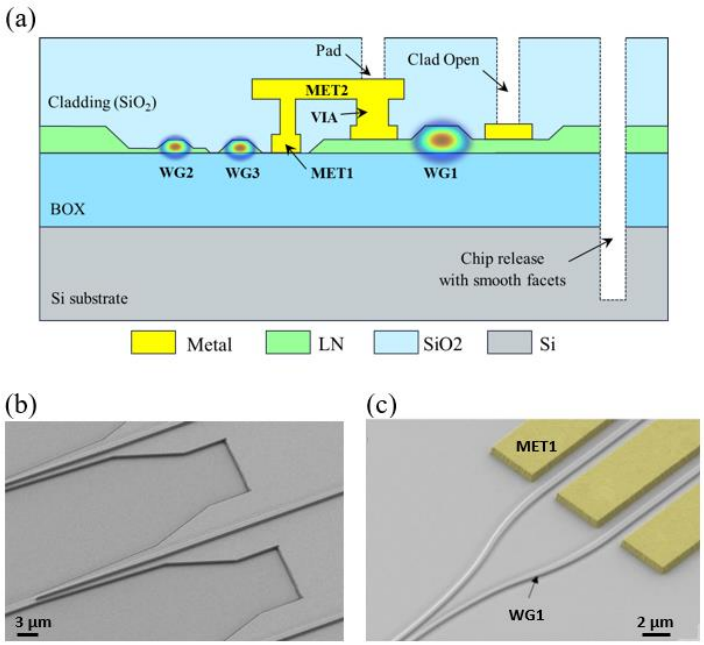

Figure 1. (a) Cross-section of the TFLN platform. SEM images of edge couplers (b) and MZM (c).

3. STANDARD ELECTRO-OPTICAL MODULATOR

Figure 2 shows a schematic of the setup used for the RF characterization of the modulators. Light from a mode hop free laser emitting at 1550 nm is sent to the chip through a polarization controller, which selects TE polarization, and a lensed fiber. A DC bias is applied to drive the modulator at the quadrature point. An RF signal is generated by a VNA and applied to the electrodes through ground-signal-ground electrical probes. The optical output is recorded by a fast photodetector. For DC measurements, a triangular electrical signal with a frequency of 5 kHz is directly applied to the electrodes, and the modulated optical output is recorded by a photodetector, whose response is acquired using a 500 MHz bandwidth oscilloscope.

The layout of our standard MZM demonstrating the technology layers is presented in Figure 3(a). The circuit encompasses a series of optimized building blocks from the PDK, such as MMI beam splitters, waveguide crossing, and edge couplers [7, 8]. We adopted a push-pull configuration for the electrodes with a pair of ground-signal-ground pads to minimize the half-wave voltage and facilitate the high-speed probing. For designing the MZM, simulations have been conducted to achieve a 50-ohm match condition for the modulator, considering the specific dimensions of the layers provided by the platform criteria. A signal electrode width of 13.7 µm and a signal gap of 4.5 µm were chosen to balance optical and RF losses while also ensuring optical and RF phase matching and an efficient electric field distribution across the electrodes. This approach guarantees the modulator's high-speed functionality with low power consumption.

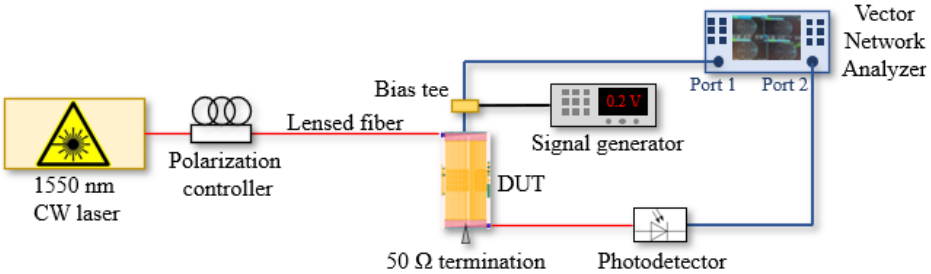

Figure 2. Sketch of the setup used for RF EO measurements.

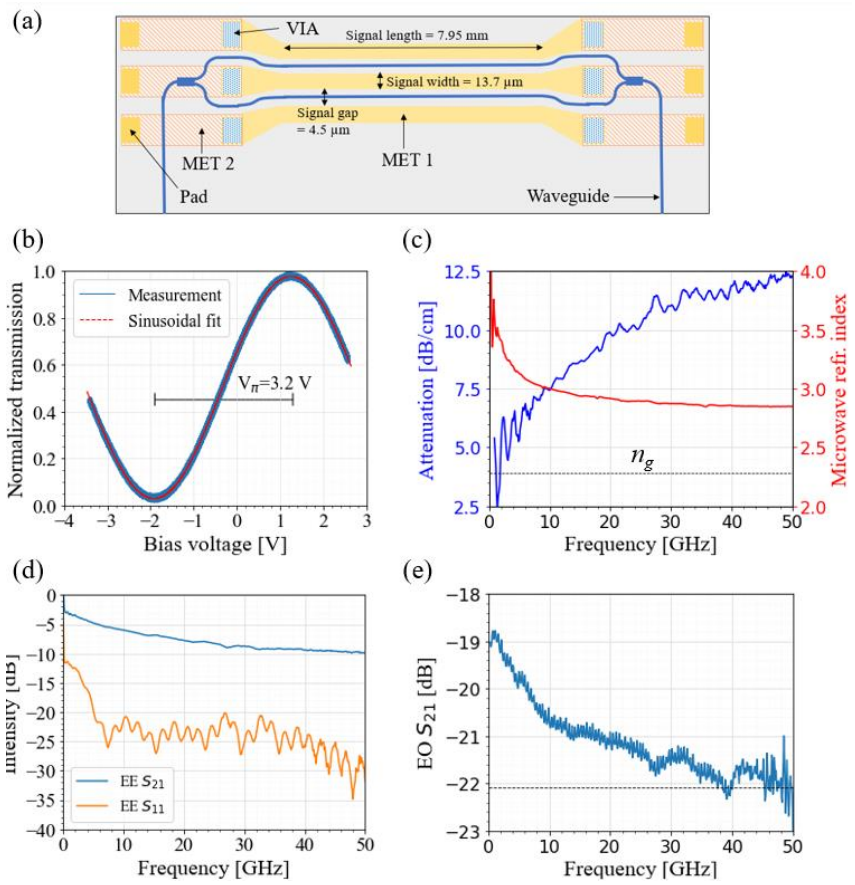

Figure 3. (a) Schematics of the standard MZM. (b) Measured modulated optical response. (c) Measured attenuation (blue curve) and microwave refractive index (red curve) as a function of RF frequency. Measured electrical (d) and electro-optical (e) response.

The modulated optical response of a MZM with a signal length of 7.95 mm is shown in Figure 3(b). The modulator exhibits a half-wave voltage of 3.26 V, an extinction ratio of 15.4 dB, and total device insertion loss (including fiber-to-chip and chip-to-fiber coupling loss) of 9.8 dB. In the RF domain, the relatively low electrical signal attenuation (Figure 3(c), blue curve) allows to achieve high EE bandwidth (Figure 3(d), blue curve), as the transmitted signal power decreases of about 6 dB at 50 GHz as compared to its value at the 1 GHz reference frequency. The microwave refractive index extracted from measurements is around 2.85 at high frequency (Figure 3(c), red curve). This value is close to the optical group index of 2.28 retrieved from simulations (black dashed line in Figure 3(c)), yet the not perfect matching between the microwave and optical waves speed is a limiting factor for the modulator's EO performances at high frequency. This aspect will be addressed in future design to further improve the performances of the device. The low electrical signal reflection (below 20 dB, see Figure 3(d), orange curve) indicates a good impedance mismatch. Finally, Figure 3(e) shows the EO frequency response. The bandwidth exceeds 50 GHz, given that the output power hasn't decreased by 3 dB at this frequency (black dashed line, calculated relatively to 1 GHz). These findings highlight the device's significant potential to operate beyond 50 GHz bandwidth, a crucial milestone for required modulation schemes. Further refinements could focus on improving the metals quality to reduce the electrical losses, and to adjusting the modulator dimensions for a better microwave-optical refractive index matching. These improvements could increase the bandwidth even further, potentially beyond 100 GHz.

4. FOLDED ELECTRO-OPTICAL MODULATORS

To be able to drive a modulator with fully integrated CMOS electrical circuits, the modulator's half-wave voltage should be at the 1 V level. However, it is widely recognized that there exists an inverse relationship between the length of an electro-optic (EO) modulator and its half-wave voltage. While this design principle tempts designers to decrease the modulator's operating voltage by increasing its length, such a strategy comes at the cost of increased chip area, higher insertion loss, and a well-known phase mismatch with the microwave during high-speed operations. In applications within

the DC domain, the primary concern lies in delivering a design with minimal optical loss and a compact footprint. A clever workaround to accommodate a lengthy EO device within a confined area is to employ folding techniques [9,10]. This can be achieved through strategic utilization of waveguide crossings and the incorporation of two levels of metallization layers to ensure efficient operation. The layout of a typical folded MZI modulator demonstrating our technology layers is presented in Figure 4 (a). The basic structure (e.g. beam splitter, signal gap, signal width) is identical to the one of the standard modulator. In this case, however, the optical arms and the electrodes undergo several 180° turns, allowing to increase the signal length while keeping the design compact. It is worth noticing that implementation of an on-chip folded modulator architecture without two-levels of metallization would be very challenging and inefficient in terms of the modulators actuation and the optical loss budget. One could still implement a similar architecture using a single metal layer and add a back end of line processing to make required electrical connections. Indeed, the push-pull configuration requires waveguide crossing at the U-turns, and two metallization levels connected through a via are essential to avoid covering the waveguides with metallization, which would lead to high losses.

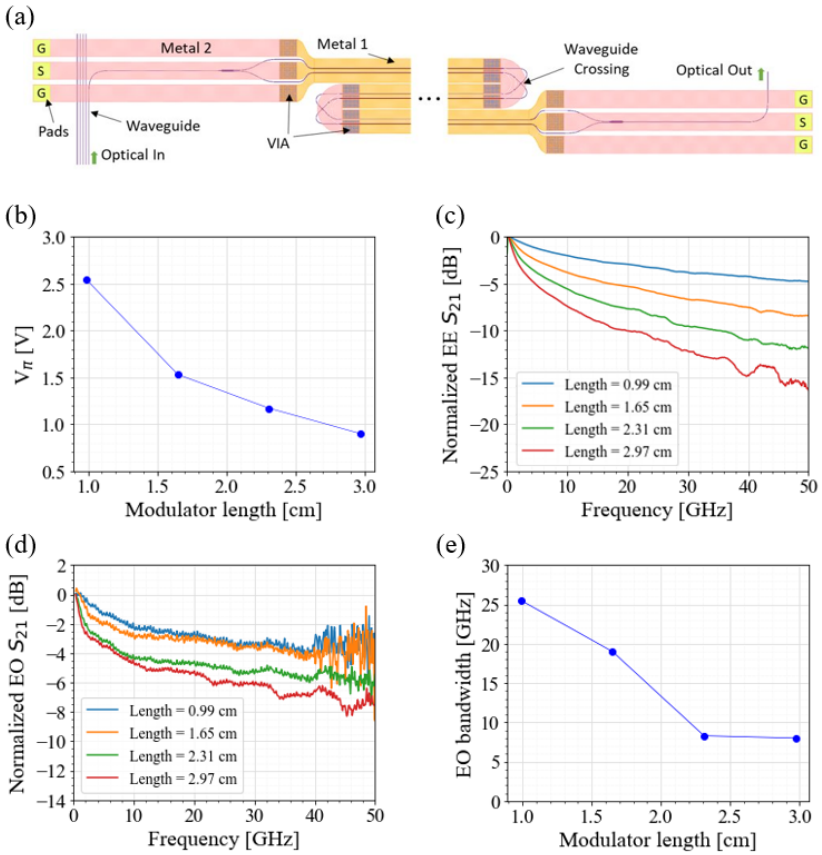

Figure 4. (a) Schematics of the folded MZM. (b) Measured half-wave voltage as a function of the modulator length. Measured electrical (c) and electro-optical (d) response of modulators of different lengths. (e) Measured EO bandwidth as a function of the modulator length.

Figure 4(b) shows the measured half-wave voltage of four folded modulators as a function of their length. As expected, V_π decreases with the length, highlighting the importance of the folded design to achieve low V_π in a compact chip. The insertion losses are between 12 and 14 dB, slightly increasing for longer modulators, but mainly driven by fiber-to-chip and chip-to-fiber coupling losses (ca 4 dB/facet). The extinction ratio is above 12 dB for all modulators. In addition, the 29.7 mm long modulator exhibits a V_π of 0.9 V. This value falls withing the CMOS-level-voltage operation that brings a substantial advantage for the EO modulator enabling to drive the device with fully integrated CMOS electrical circuits, without the need of off-chip amplification. Thanks to our folded modulator design, we achieved such value in a compact 5mm × 5mm chip. Figures 4(c) and 4(d) show the electrical and electro-optical response of the modulators, respectively. An EO bandwidth higher than 25 GHz and 8 GHz is achieved in the shortest and longest modulators respectively. More advanced designs, like slotted electrodes [11] and improvement in the fabrication process could help in reducing optical

and microwave losses and further phase match the optical and RF fields, enhancing the efficiency in terms of the operating voltage and the bandwidth.

5. CONCLUSION

We presented the EO characterization of standard and folded MZMs manufactured in a TFLN PICs foundry following design rules and operating in the telecom C-band. The standard modulator exhibits an EO bandwidth beyond 50 GHz, whereas the folded modulators represent a valuable option for voltage-level operation in a compact design. This holds great potential for low-power integrated EO circuits seamlessly interfacing with CMOS electrical circuits, which could have been of interest for various applications such as in programmable photonics. The two metal layers greatly facilitate the design of intricate PIC components within the TFLN PIC platform. Furthermore, availability of multi-level metallization technology in a standardized PIC platform promises for facile electrical interfacing of the TFLN PICs for standard packaging approaches. The success of this device serves as a validation of our standard fabrication process. According to the increasing demand for low power, high bandwidth photonic devices, developing reliable manufacturing of TFLN PICs in a standardized platform will potentially pave the way for fast, large-scale, and energy-efficient PIC systems.

ACKNOWLEDGEMENTS

This project has received funding from the European Union's Horizon 2020, GA No. 101016138; European Union Horizon under GA Nos. 101070506, 101070441 and 101070581.

REFERENCES

[1] D. Zhu *et al*., "Integrated photonics on thin-film lithium niobate," Adv. Opt. Photon. 13(2), 242-352 (2021). https://doi.org/10.1364/AOP.411024
[2] A. Liu *et al*., "High-speed optical modulation based on carrier depletion in a silicon waveguide," Opt. Express 15(2), 660-668 (2007). https: //doi.org/10.1364/OE.15.000660
[3] N. C. Harris *et al*., "Efficient, compact and low loss thermo-optic phase shifter in silicon," Opt. Express 22(9), 10487-10493 (2014). https://doi.org/10.1364/OE.22.010487
[4] C. Errando-Herranz *et al*., "MEMS for Photonic Integrated Circuits," IEEE Journal of Selected Topics in Quantum Electronics 26(2), 1-16 (2020). https: //doi.org/10.1109/JSTQE.2019.2943384
[5] A. Melikyan *et al*., High-speed Plasmonic Modulators," Nature Photonics 8, 229-233 (2014). https://doi.org/10.1038/nphoton.2014.9
[6] M. Zhang *et al*., Integrated lithium niobate electro-optic modulators: when performance meets scalability," Optica 8(5), 652-667 (2021). https://doi.org/10.1364/OPTICA.415762
[7] J. Leo *et al*., "Wafer-scale fabrication of low-loss waveguides in lithium niobate on insulator (LNOI) integrated photonics platform," European Conference on Optical Communication, Basel (2022).
[8] A. Monney *et al*., "Statistical characterization of MMI beam splitters on thin film lithium niobate on insulator (LNOI) platform at telecom wavelength," Conference on Lasers and Electro-Optics/Europe and European Quantum Electronics Conference, Munich (2023).
[9] S. Sun *et al*., "Folded Heterogeneous Silicon and Lithium Niobate Mach–Zehnder Modulators with Low Drive Voltage," Micromachines 12, 823 (2021). https://doi.org/10.3390/mi12070823
[10] J. Hu *et al*., "Folded thin-film lithium niobate modulator based on a poled Mach–Zehnder interferometer structure," Opt. Lett. 46, 2940-2943 (2021). https://doi.org/10.1364/OL.426083
[11] P. Kharel *et al*., "Breaking voltage–bandwidth limits in integrated lithium niobate modulators using micro-structured electrodes," Optica 8, 357-363 (2021). https://doi.org/10.1364/OPTICA.416155